

Shape Optimization and Sensitivity Analysis for Triply Periodic Minimal Surface Lattice Structures Under Periodic Boundary Conditions

Chongyi Wei, Douglas E Smith*

Department of Mechanical Engineering, Baylor University, Waco, TX 76706

* Corresponding author: douglas_e_smith@baylor.edu

Abstract

Lattice structures have drawn increased attention due to the advance of additive manufacturing making it possible to fabricate these geometrically complex periodic structures. The widely-adopted Triply Periodic Minimal Surface (TPMS) lattice are formed from predefined level set functions having a single tunable parameter that defines the lattice geometry but lacks design flexibility. This paper develops a radial basis function-based shape optimization technique to modify the shape of TPMS lattice for improved structural performance. The finite element-based shape sensitivity analysis used in the optimization is derived by both direct differentiation and adjoint variable methods where special attention is given to periodic boundary conditions in the formulation that updates the nodal locations while preserving the advantages of smooth varying surface and cubic symmetric properties of TPMS. Scaffold or sheet TPMS lattice Representative Volume Element (RVE) are optimized to for minimal strain energy and minimum anisotropy under von Mises stress and volume constraints.

1. Introduction

Spatially varying design of triply periodic minimal surface (TPMS) lattice structures have continued to gain interest among researchers, particularly as related to varying relative density [1], hybrid functionality [2], non-uniform thickness structures [3], and varying lattice orientations [4] for a wide range of lattice structures. Design schemes have been implemented at the macroscale to tune mechanical performance with mesoscale design variables such as relative cell density and orientation, where the transition between lattice unit cells is accomplished by interpolation or by solving intermediate mapping functions [4]. However, these methods lack broader shape control of the unit cell that is often treated as a Representative Volume Element (RVE). For instance, minimization of stress concentration [5] or homogenized anisotropy [3] is of importance for the fabrication of additive manufacturing and practical application but have yet to receive significant attention .

TPMS unit cell design has been performed where the prior research has focused on tuning effective material properties for sheet-based TPMS lattice structures [6]. Ad hoc modification of TPMS lattice structures has been proposed for bone substitutes which resulted in improved

stiffness and strength [7], the time-consuming grid search of modification parameters in this earlier work is employed for computing the optimal solution. Shape optimization has emerged as an ideal candidate for tailoring mechanical performance by adjusting local geometry in a prescribed manner to satisfy specified structural requirements. For example, the open-cell variable thickness TPMS shell lattice was optimized under a strain energy-based optimization algorithm to reduce the elastic anisotropy [8]. Similarly, a non-uniform thickness TPMS sheet lattices were designed to improve an elastic isotropy with underlying anisotropic constitutive materials, where the universal anisotropy index was applied to lattices with cubic symmetry [3]. TPMS shell mid-surfaces have also been designed where a B-spline parameterized Monge patch was defined to maintain cubic symmetry and simplify sensitivity evaluations [9]. Unfortunately, surface patches parameterized by a single variable lacks the ability to model more complicated geometry variations, especially for Gyroid or Diamond TPMS surfaces with Bonnet transformation [10]. The fundamental surface patch is duplicated and transformed to generate the complete Gyroid TPMS lattice, where many NURBS patches are employed to model complex geometry [11]. It has been shown that cracks can arise at the seams when deforming a surface made of NURBS patches [12]. Additionally, periodic boundary conditions that ensure the tessellation of lattice structures [3] must apply to all external surfaces of the TPMS RVE rather than being limited to a subregion of the unit cell.

In the current work, a finite element-based shape optimization is proposed to minimize either the strain energy or an anisotropy index subject to von Mises stress and volume constraints. We define radial basis functions to modify the shape of both sheet and scaffold-based TPMS structures which avoid cumbersome geometry parametrization. Explicitly constructed surface patches are iteratively updated by modifying their surface location or thickness distribution for the scaffold or sheet-based TPMS lattice structures, respectively. More importantly, special attention is given to the periodic boundary conditions that ensure periodic symmetry in the proposed approach which includes elemental node coupling. Design velocities are defined in terms of the radial basis functions to provide a means for computing the design gradients used to change the shape of the TPMS surface during the optimization process. Design sensitivities that evaluate the derivative of design metrics with respect to shape design variables are computed using the adjoint variable method where special attention is given to imposed periodic boundary conditions. Details given here present calculations for defining TPMS finite element models, derivation of the design sensitivities, and example TPMS shape optimization problems under periodic boundary conditions.

2. Defining TPMS lattice structures and TPMS shape change

TPMS geometries may be implicitly defined by a universal formulation in terms of reciprocal vectors through [4,10]

$$\Psi(\mathbf{r}) = \sum_{m=1}^M \mu_m \cos((\mathbf{h}_m \cdot \mathbf{r} + p_m)) + t \quad (1)$$

where μ_m is the m -th periodic amplitude, \mathbf{h}_m is the m -th reciprocal vector, p_m is phase shift, \mathbf{r} is the position vector, t is the level set value, and M is the number of terms that compose TPMS level set function Ψ . The explicit TPMS geometry can be extracted from the level set function in Eqn. 1 and discretized into finite elements within the design domain for structural analysis of the TPMS unit cell (see e.g. [1]). Additionally, we use the geometry described by Eqn. 1 to define the initial design domain for our TPMS optimizations. Shape optimization requires that the nodal locations that form the finite element mesh be defined by design parameters. Here we calculate modified nodal locations defined by X_m from the initial discretized domain X_0 as [7]

$$X_m(\mathbf{x}) = X_0(\mathbf{x}) + F_{RBF}(\mathbf{x}) = X_0(\mathbf{x}) + N_0 \sum_{i=1}^{np} b_1 \exp(-b_2 \|\mathbf{x} - \bar{\mathbf{x}}_s^i\|) \quad (2)$$

where \mathbf{x} denotes the coordinates of any point forming the discretized design domain X_0 , F_{RBF} is radial basis function, N_0 represents the surface nodal normal on the initial design domain, b_1 and b_2 are design variables that modify the domain shape, $\|\mathbf{x} - \bar{\mathbf{x}}_s^i\|$ denotes the Euclidean distance between the design domain and control point $\bar{\mathbf{x}}_s^i$ ($\bar{\mathbf{x}}_s^i$ is the i -th column vector from $\bar{\mathbf{x}}_s$). The control nodes modify local TPMS geometry and are close to the surface of TPMS lattice structures shown as Fig. 1 which distribute symmetrically inside the RVE and given as

$$\bar{\mathbf{x}}_s = b_3 \begin{bmatrix} 1 & -1 & -1 & 1 & 1 & -1 & 1 & -1 \\ 1 & -1 & 1 & -1 & -1 & 1 & 1 & -1 \\ 1 & -1 & 1 & -1 & 1 & -1 & -1 & 1 \end{bmatrix} \quad (3)$$

where b_3 changes the location of control points resulting in varying modification inside RVE diagonally on lattice geometry, np is the column number of $\bar{\mathbf{x}}_s$ or the number of control points.

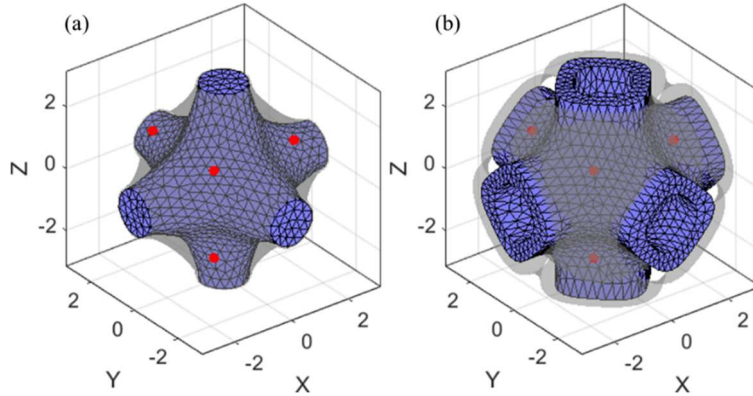


Figure 1. The modified scaffold-based (a) and sheet-based (b) Primitive TPMS lattice with control points demonstration (control points move inside RVE by changing b_3 and are marked as red solid circle)

We define the design velocity V_i from perturbation can be defined as

$$F_{RBF}(b_i + \delta b_i) = F_{RBF}(b_i) + \delta b_i V_i \quad \text{with} \quad V_i(b_i) = \partial F_{RBF} / \partial b_i \quad (4)$$

where δ is the perturbed step size.

3. Sensitivity analysis under periodic boundary conditions

Periodic boundary conditions are imposed by defining nc displacement constraint between nodes on opposing sides of the RVE written as

$$\mathbf{u}_k^+ - \mathbf{u}_k^- = \bar{\boldsymbol{\varepsilon}}(\mathbf{x}_k^+ - \mathbf{x}_k^-), \quad k = 1, \dots, nc \quad (5)$$

where \mathbf{u}_k^+ and \mathbf{u}_k^- are the displacements on opposing sides for the k -th constraint equation (i.e., on the positive and negative surfaces, respectively) of the RVE, $\bar{\boldsymbol{\varepsilon}}$ defines the imposed macroscopic strain and $(\mathbf{x}_k^+ - \mathbf{x}_k^-)$ is the distance between opposing nodes on the RVE faces. For a quadrilateral element e located on the positive boundary of the RVE, its displacement vector \mathbf{u}_e^+ may be partitioned as

$$\mathbf{u}_e^+ = \begin{bmatrix} \mathbf{u}_1 \\ \mathbf{u}_2 \\ \mathbf{u}_3 \\ \mathbf{u}_4 \end{bmatrix} = \begin{bmatrix} \mathbf{u}_1^- + \tilde{\boldsymbol{g}} \\ \mathbf{u}_2^- + \tilde{\boldsymbol{g}} \\ \mathbf{u}_3 \\ \mathbf{u}_4 \end{bmatrix} = \mathbf{L}_e \tilde{\mathbf{u}}_e + \tilde{\boldsymbol{g}}_e \quad (6)$$

where $\tilde{\boldsymbol{g}}_e$ is the contribution of $\bar{\boldsymbol{\varepsilon}}(\mathbf{x}_i^+ - \mathbf{x}_i^-) = \tilde{\boldsymbol{g}}$ for element lying on boundary and composing periodic boundary conditions, $\tilde{\mathbf{u}}_e = [\mathbf{u}_1^- \quad \mathbf{u}_2^- \quad \mathbf{u}_3 \quad \mathbf{u}_4]^T$ is the reduced element vector of degree of freedom, \mathbf{L}_e is the mapping matrix which transforms element displacement vector \mathbf{u}_e^+ into the constrained $\tilde{\mathbf{u}}_e$ and couples degrees of freedom for the periodic boundaries, \mathbf{u}_1^- and \mathbf{u}_2^- are displacement vector on the negative surface. The finite element equilibrium equations $\sum_e \delta \mathbf{u}_e^T (\mathbf{K}_e \mathbf{u}_e - \mathbf{F}_e) = 0$, where $\delta \mathbf{u}_e$ is the arbitrary virtual displacement, \mathbf{K}_e is the element stiffness matrix, \mathbf{F}_e is the element force vector, are modified to incorporate the periodic boundary conditions as

$$\sum_e \delta \tilde{\mathbf{u}}_e^T \mathbf{L}_e^T \mathbf{K}_e \mathbf{L}_e \tilde{\mathbf{u}}_e - \sum_e (\delta \tilde{\mathbf{u}}_e^T \mathbf{L}_e^T \mathbf{F}_e - \delta \tilde{\mathbf{u}}_e^T \mathbf{L}_e^T \mathbf{K}_e \tilde{\boldsymbol{g}}_e) = 0 \quad (7)$$

where \sum_e denotes the assembly of finite element stiffness matrices and load vectors. The resulting modified stiffness matrix $\tilde{\mathbf{K}}_e$ and force vector $\tilde{\mathbf{F}}_e$ from the finite element analysis are defined as $\tilde{\mathbf{K}}_e = \mathbf{L}_e^T \mathbf{K}_e \mathbf{L}_e$ and $\tilde{\mathbf{F}}_e = \mathbf{L}_e^T (\mathbf{F}_e - \mathbf{K}_e \tilde{\boldsymbol{g}}_e)$, respectively. For elements without degrees of freedom on the periodic boundaries of the RVE, \mathbf{L}_e simply reduces to the identity matrix.

3.1. Optimization formulation and analytical sensitivity analysis

Our TPMS shape optimizations is conducted by solving the design optimization problem stated as

$$\left\{ \begin{array}{l} \min \\ \text{s. t.} \end{array} \right. \left\{ \begin{array}{l} f(\mathbf{b}) = \frac{1}{2} \sum_{l=1}^N \mathbf{u}_l^T \mathbf{K}_l \mathbf{u}_l \\ g(\mathbf{b}) = \left(\sum_{l=1}^N \sigma_{vm}^p \right)^{1/p} = \sigma_{pn} \leq \sigma_{vm}^0 \\ \sum_e (\tilde{\mathbf{K}}_e \tilde{\mathbf{u}}_e - \tilde{\mathbf{F}}_e) = 0 \\ V_{min} \leq \left\{ V_{tot} = \sum_{l=1}^N V_l(\mathbf{b}) \right\} \leq V_{max} \\ b_{min} \leq b_i \leq b_{max}, \quad i = 1 \dots n \end{array} \right. \quad (8)$$

where $f(\mathbf{b})$ is the strain energy objective function, \mathbf{b} is the vector of design variables, n is the number of design variables, b_{min} and b_{max} are lower and upper bounds for the design variables, respectively, N is the number of finite elements, $g(\mathbf{b})$ is the p -norm von Mises stress constraint, σ_{vm} is the von Mises stress, $\sum_e (\tilde{\mathbf{K}}_e \tilde{\mathbf{u}}_e - \tilde{\mathbf{F}}_e) = 0$ is the finite element state equation under periodic boundary conditions from Eqn. 7, V_l is the volume for each element, V_{min} and V_{max} are lower and upper bound for volume constraints, respectively. The p -norm von Mises stress constraint g transform the local stresses into a global stress function which limits the maximum stress [13].

We use a gradient-based optimization algorithm to solve Eqn. 8, where accurate and efficient sensitivity analyses are required when using the TPMS finite element solutions [14]. Errors in the sensitivity analysis will yield inaccurate results or a distorted finite element mesh and thus fail in achieving an optimal solution [15]. The design sensitivity of the functions f , or g in Eqn. 8) with respect to design variables \mathbf{b} is calculated using the chain rule as, $dF/d\mathbf{b} = (\partial F/\partial \tilde{\mathbf{u}})(\partial \tilde{\mathbf{u}}/\partial \mathbf{b}) + \partial F/\partial \mathbf{b}$, the difficulties for evaluating $df/d\mathbf{b}$ arises from the presence of the implicit sensitivity response $\partial \tilde{\mathbf{u}}/\partial \mathbf{b}$, $\partial \tilde{\mathbf{u}}_e/\partial \mathbf{b}$ must be evaluated by direct differentiation or eliminated by adjoint method from the equilibrium equation in Eqn. 7 [16]. In the direct differentiation method, a pseudo problem is formed for the i -th design variable by differentiating Eqn. 7 by the design variable b_i as

$$\sum_e \left(\frac{\partial \tilde{\mathbf{K}}_e}{\partial b_i} \tilde{\mathbf{u}}_e(b_i) + \tilde{\mathbf{K}}_e \frac{d\tilde{\mathbf{u}}_e(b_i)}{db_i} - \frac{\partial \tilde{\mathbf{F}}_e(b_i)}{\partial b_i} \right) = 0 \quad (9)$$

Recalling that \mathbf{L}_e and $\tilde{\mathbf{g}}_e$ are a constant matrix and vector, respectively, from Eqn. 6, differentiation of $\tilde{\mathbf{K}}_e$ and $\tilde{\mathbf{F}}_e$ gives $\frac{\partial \tilde{\mathbf{K}}_e(b_i)}{\partial b_i} = \mathbf{L}_e^T \frac{\partial \mathbf{K}_e}{\partial b_i} \mathbf{L}_e$ and $\frac{\partial \tilde{\mathbf{F}}_e(b_i)}{\partial b_i} = \mathbf{L}_e^T \frac{\partial \mathbf{K}_e}{\partial b_i} \mathbf{L}_e - \frac{\partial \mathbf{K}_e}{\partial b_i} \tilde{\mathbf{g}}_e$, respectively.

3.2 Adjoint variable method for sensitivity analysis

In the adjoint variable method, we eliminate the implicit response $d\mathbf{u}_e(b_i)/db_i$ in Eqn. 9. This is accomplished by employing the Lagrange multiplier method, which effectively treats the

finite element equilibrium equations Eqn. 7 as equality constraints. We first combine objective function from Eqn. 8 with Eqn. 7 to define the augmented function

$$\hat{f} = f(\mathbf{u}(\mathbf{b}), \mathbf{b}) - \tilde{\boldsymbol{\lambda}}(\mathbf{b})^T \sum_e (\tilde{\mathbf{K}}_e \tilde{\mathbf{u}}_e - \tilde{\mathbf{F}}_e) \quad (10)$$

where $\tilde{\boldsymbol{\lambda}}(\mathbf{b})$ is the adjoint vector and is an arbitrary vector with a length equal to the number of degrees of freedom in the finite element system. Since $\sum_e (\tilde{\mathbf{K}}_e \tilde{\mathbf{u}}_e - \tilde{\mathbf{F}}_e) = 0$ from Eqn. 7, $\hat{f} = F(\mathbf{u}(\mathbf{b}), \mathbf{b})$. Differentiation of Eqn. 10 with respect to the design variable b_i gives

$$\begin{aligned} \frac{d\hat{f}}{db_i} &= \frac{\partial f}{\partial \mathbf{u}} \frac{d\mathbf{u}}{db_i} + \frac{\partial f}{\partial b_i} - \frac{d\tilde{\boldsymbol{\lambda}}^T}{db_i} \sum_e (\tilde{\mathbf{K}}_e \tilde{\mathbf{u}}_e - \tilde{\mathbf{F}}_e) \\ &\quad - \tilde{\boldsymbol{\lambda}}^T \sum_e \left(\frac{\partial \tilde{\mathbf{K}}_e}{\partial b_i} \tilde{\mathbf{u}}_e + \tilde{\mathbf{K}}_e \frac{d\tilde{\mathbf{u}}_e}{db_i} - \frac{\partial \tilde{\mathbf{F}}_e}{\partial b_i} \right) \end{aligned} \quad (11)$$

where $d\hat{f}/db_i = df/db_i$ since the terms multiplying $\partial \tilde{\boldsymbol{\lambda}}/b_i$ and $\tilde{\boldsymbol{\lambda}}$ both are equal to zero from Eqn. 7 and 9, respectively. The above differentiation can be rearranged as

$$\frac{d\hat{f}}{db_i} = \frac{\partial f}{\partial b_i} - \sum_{k=1}^N \tilde{\boldsymbol{\lambda}}_k^T \left(\frac{\partial \tilde{\mathbf{K}}_k}{\partial b_i} \tilde{\mathbf{u}}_k - \frac{\partial \tilde{\mathbf{F}}_k}{\partial b_i} \right) + \sum_e \left(\frac{d\mathbf{u}_e^T}{db_i} \frac{\partial f_e^T}{\partial \mathbf{u}_e} - \frac{d\tilde{\mathbf{u}}_e^T}{db_i} \tilde{\mathbf{K}}_e^T \tilde{\boldsymbol{\lambda}}_e \right) \quad (12)$$

Combining Eqn. 12 with $d\mathbf{u}_e(b_i)/db_i = \mathbf{L}_e d\tilde{\mathbf{u}}_e(b_i)/db_i$ from Eqn. 6, $d\mathbf{u}_e(b_i)/db_i$ in Eqn. 12 can be eliminated with $d\tilde{\mathbf{u}}_e(b_i)/db_i$, resulting in Eqn. 12 written as

$$\frac{d\hat{f}}{db_i} = \frac{\partial f}{\partial b_i} - \sum_{k=1}^N \tilde{\boldsymbol{\lambda}}_k^T \left(\frac{\partial \tilde{\mathbf{K}}_k}{\partial b_i} \tilde{\mathbf{u}}_k - \frac{\partial \tilde{\mathbf{F}}_k}{\partial b_i} \right) + \sum_e \frac{d\tilde{\mathbf{u}}_e^T}{db_i} \left(\mathbf{L}_e^T \frac{\partial f_e^T}{\partial \mathbf{u}_e} - \tilde{\mathbf{K}}_e^T \tilde{\boldsymbol{\lambda}}_e \right) \quad (13)$$

where $\tilde{\boldsymbol{\lambda}}_e$ is the elemental adjoint vector, \mathbf{L}_e couples the degree of freedom for each element lying on the periodic boundaries, $\partial f/\partial b_i$ and $\partial f_l/\partial \mathbf{u}_l$ are the explicit sensitivity response of objective function respect to design variables and nodes displacement, defined as $\frac{\partial f}{\partial b_i} = \frac{1}{2} \sum_{l=1}^N \left(\mathbf{u}_l^T \frac{\partial \mathbf{K}_e}{\partial b_i} \mathbf{u}_l \right)$ and $\frac{\partial f_l}{\partial \mathbf{u}_l} = \left(\mathbf{u}_l^T \frac{\partial \mathbf{K}_l}{\partial b_i} \right)$, respectively. Since the adjoint vector $\tilde{\boldsymbol{\lambda}}$ is arbitrary, it may be selected to eliminate the term multiplying the implicit response sensitivity $\partial \tilde{\mathbf{u}}_e/b_i$. The resulting adjoint problems becomes

$$\sum_e \left(\tilde{\mathbf{K}}_e^T \tilde{\boldsymbol{\lambda}}_e - \mathbf{L}_e^T \frac{\partial f_e^T}{\partial \mathbf{u}_e} \right) = 0 \quad (14)$$

The adjoint variable $\tilde{\boldsymbol{\lambda}}$ is computed by assembling the adjoint load $\frac{\partial f}{\partial \mathbf{u}} \mathbf{L}_e$ and solving the system of equations as Eqn. 14. After the adjoint vector is computed, the design sensitivity df/b_i

is calculated for each design variable as shown in Eqn. 13. Similarly, the adjoint vector $\tilde{\boldsymbol{\gamma}}$ for p-norm von Mises constraint can be formulated as

$$\sum_e \left(\tilde{\mathbf{K}}_e^T \tilde{\boldsymbol{\gamma}}_e - \mathbf{L}_e^T \frac{\partial g_l^T}{\partial \mathbf{u}_l} \right) = 0 \quad (15)$$

where $\tilde{\boldsymbol{\gamma}}_e$ is the elemental adjoint vector, g_l is the elementary contribution of p-norm von Mises stress. Furthermore, the adjoint method for homogenization can be derived from a similar process, the elasticity matrix can be obtained by average stress and strain vectors, which may be employed to minimize the homogenized anisotropy for lattice structures.

4. Results and discussion

4.1. Validation of the sensitivity analysis using finite difference derivatives

The sensitivity analysis calculations for df/db_2 and df/db_3 given above are validated here using the finite difference (FD) method where results appear in Table 1. Analytical sensitivity from direct differentiation method (using a finite difference step to get the design velocities) and the forward finite difference method are compared over a range of finite difference step size. The step size 1.0E-5 to 1.0E-6 shows best agreement between the analytical sensitivity analysis and finite difference method. As expected, inaccurate sensitivities result from either too large or too small of a step size for the finite difference approach. However, direct analytical sensitivity always shows a good sensitivity response when the step size is smaller than 1E-3 in the design velocity calculation.

Table 1. The sensitivity for strain energy for Primitive sheet-based TPMS lattice structure

δ	Analytical b_2	FD b_2	Analytical b_3	FD b_3
1.0E-1	-10.763836	-10.763858	18.021497	18.021297
1.0E-2	-11.872698	-11.872701	17.432766	17.432751
1.0E-3	-11.992244	-11.992240	17.320946	17.320949
1.0E-4	-12.004291	-12.004282	17.309343	17.309333
1.0E-5	-12.005496	-12.005283	17.308178	17.308304
1.0E-6	-12.005617	-12.005912	17.308062	17.310958
1.0E-7	-12.005629	-11.990778	17.308050	17.315615
1.0E-8	-12.005630	-12.223609	17.308049	17.229468
1.0E-9	-12.005631	-6.519258	17.308049	17.229468
1.0E-10	-12.005623	-116.415322	17.308047	18.626451
1.0E-11	-12.005574	139.698386	17.308063	279.396772
1.0E-12	-12.005967	-3026.798368	17.308932	-3725.290298

The direct differentiation and adjoint variable method show the same sensitivity response under same design velocity as Table 1.

To better understand the difference between those two approaches for sensitivity analysis, the $d\mathbf{u}/db_i$ are visualized as shown in Fig. 2 on the finite element mesh since they are the same size with nodal displacement \mathbf{u} , the implicit terms are symmetric around the orthotropic axes as well. The components of the adjoint vector for strain energy objective are close to a constant as shown in Fig. 3. Moreover, the adjoint load $\partial f_l/\partial \mathbf{u}_l$ on the right side of Eqn. 14 or 15 is independent design variables b_i , where λ (the same size with \mathbf{u} , which are partitioned in the same manner as \mathbf{u} as λ_x , λ_y and λ_z) is independent of design parameter b_i , specifically, λ stay unchanged for all df/db_i . Thus, it means that the adjoint vector only needs to be solved once for the given adjoint problem. However, two adjoint problems are assembled and solved for the objective functions and p -norm von Mises stress constraint for the current optimization model.

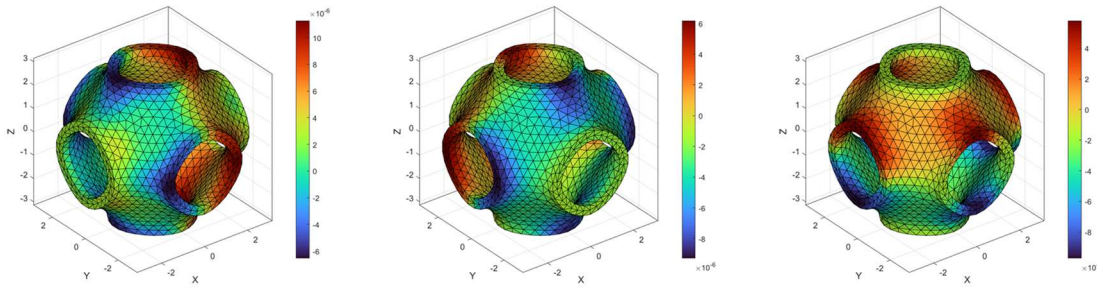


Figure 2. The visualization of $d\mathbf{u}_x/db_1$ (left), $d\mathbf{u}_y/db_2$ (middle) and $d\mathbf{u}_z/db_3$ (right) on finite element model under periodic boundary conditions for Primitive sheet-based TPMS

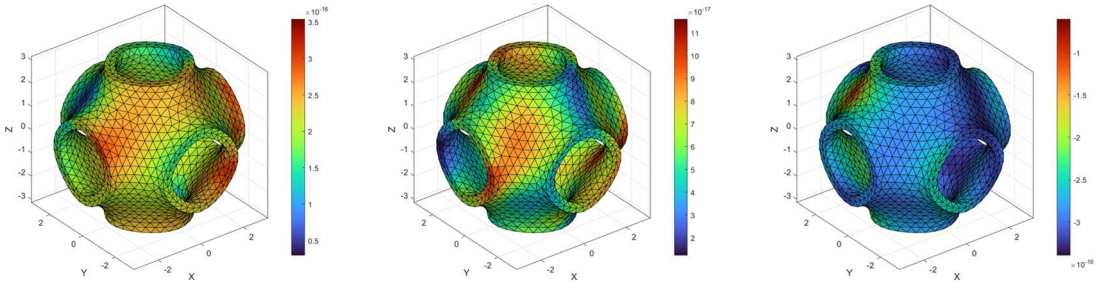


Figure 3. The visualization of $\tilde{\lambda}_x$ (left), $\tilde{\lambda}_y$ (middle) $\tilde{\lambda}_z$ (right) on finite element model under periodic boundary conditions for Primitive sheet-based TPMS

The $d\mathbf{u}/db_i$ needs to be solved for every design parameter b_i in the optimization process, but it can directly contribute to the sensitivity response of the objective function and p -norm von Mises stress constraint. Beyond that, both the adjoint variable method and direct differentiation are independent of the loading direction for TPMS with cubic symmetry, such that the x , y or z uniaxial strain enforcement produces the same sensitivity response. If there are more than two design parameters, the adjoint variable method provides a more efficient approach for sensitivity computation for Eqn. 8.

4.2. The optimization procedure

The optimization procedure and a numerical example are presented here for sheet-based Primitive TPMS lattice structures. The surface patches are first generated from the level set function Eqn. 1, and it is meshed by TetGen [17] from the MATLAB toolbox [18]. The two-surface pair composed of the sheet-based RVE are extracted, i.e., the interior and exterior surface, and the six caps on the RVE boundary are excluded which are allowed to move freely inside the corresponding plane. The perturbed design velocity is produced by the radial basis function as Eqn. 4, which modifies the coordinates of these two surface pairs along its normal direction separately. The design velocity for interior nodes is generated by solving an auxiliary elasticity problem with prescribed displacement on the design boundary [14]. Sensitivity analysis is performed by the adjoint variable method for the objective function and constraints. The method of moving asymptotes is chosen to update the design parameters [19]. The new design velocity based on the updated design parameters from the radial basis function is applied to the finite element model to acquire the optimal shape distribution.

4.3. The optimization of strain energy

The unit strain is imposed along x -axis direction by periodic boundary conditions. The initial volume for Primitive RVE is 0.194, the volume and p-norm stress constraint are 0.16 and 800 MPa, respectively, the underlying material is assumed as isotropic with Young's modulus and Poisson ratio as $2.1E11$ and 0.3, it takes 40 iterations to converge to the optimal shape distribution. The optimal shape for Primitive and its non-uniform thickness distribution (on the interior surface) are shown as Fig. 4. The optimization history is shown in Fig. 5, the normalized objective function of strain energy minimizes to 73% of its original value with 6 design parameters (with each three parameters for interior and exterior surface). Note that it reduces to 74.1% without the movable control points b_3 (cf. Eqn. 3) stays as constant. The control points (controlled by b_2 , cf. Eqn. 3) for scaffold and sheet-based TPMS lattice structures (shown as Fig. 1) may be able to move dynamically in optimization along the diagonal line inside RVE, which changes the influencing area of radial basis function on the lattice surface symmetrically. Additionally, the p-norm von Mises always satisfy the stress constraint with small variation. The proposed optimization approach may be extended to minimize the homogenized anisotropy under periodic boundary conditions, where six loading cases are considered to acquire the elasticity matrix components [5].

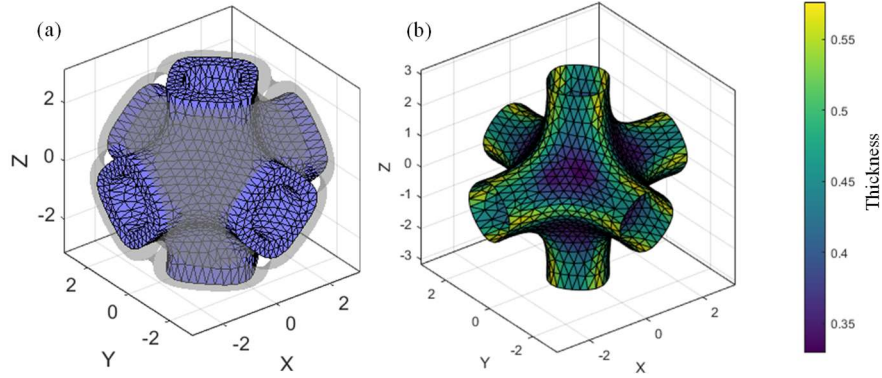


Figure 4. The optimal Primitive sheet-based TPMS lattice where gray transparent is the initial shape (a) and its non-uniform thickness distribution (b)

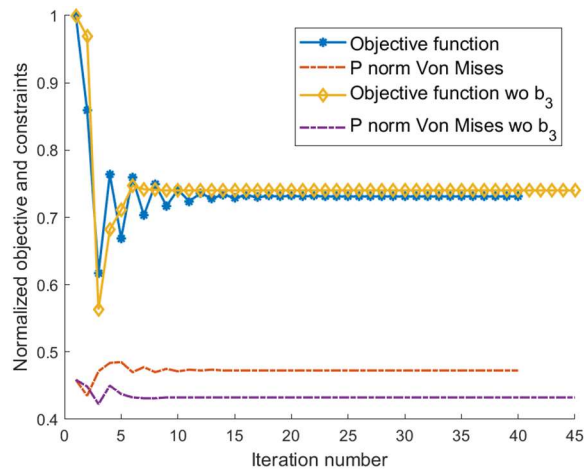


Figure 5. The optimization history for Primitive sheet-based TPMS lattice structures

4.4. The optimization of anisotropy

The second optimization model for anisotropy minimization demonstrated is implemented by the minimization of Zener index in the form of $\frac{1}{2} (Z(\mathbf{b}) - 1)^2$ rather than the strain energy from Eqn. 8, where Zener index is defined as $2C_{44}/(C_{11} - C_{12})$, and the initial conditions, volume and stress constraints keep unchanged as minimization of strain energy. The adjoint method is adopted for sensitivity analysis that is similar to derivation of strain energy objective function, where two loading cases under macroscopic strain are considered for solving the homogenized elasticity component C_{ij}^H [8,20] to compute Zener index. The iteration history is shown as Fig. 6, it takes 40 iterations to minimize the anisotropy. The spatial representation for the initial and optimized effective Young's modulus is shown in Fig. 7, where the concave sphere shape converges to the perfect sphere shape for Primitive sheet-based lattice structures. The Zener ratio

decreases from 2.108 to 1.029, where the value of 1 means isotropy and the initial and optimal shape distribution are shown as Fig. 8. The proposed minimization of anisotropy by shape optimization can be applied to other kinds of sheet TPMS lattice structures, i.e., IWP, Diamond and Gyroid, which are not shown here for limitation of space.

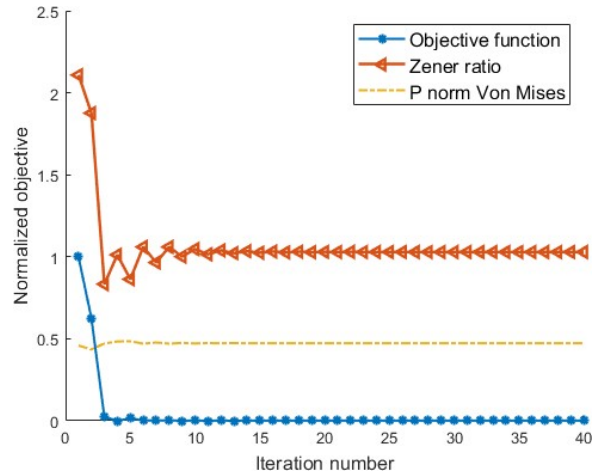


Figure 6. The optimization history for Primitive sheet-based TPMS lattice structures

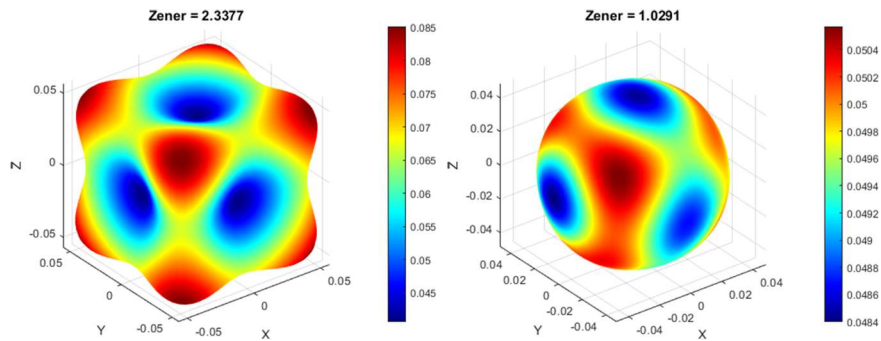


Figure 7. The initial (left) and optimal (right) spatially representation for homogenized Young's modulus for Primitive sheet-based TPMS lattice structures

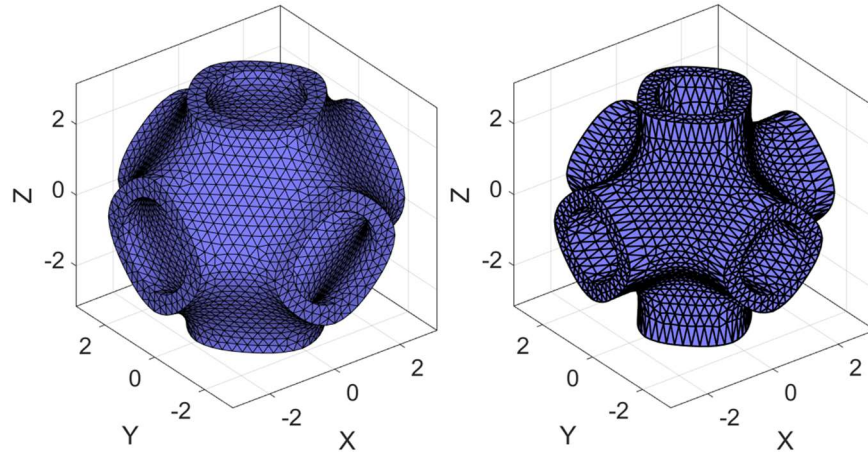


Figure 8. The initial (left) and optimal (right) shape distribution for sheet Primitive lattice structures

5. Conclusion

A radial basis function-based shape optimization approach based on finite element method for TPMS lattice structures is presented. The radial basis shape parameters are treated as design variables and directly applied to define changes to nodal coordinates along the surface normal direction for TPMS lattice structures in the finite element model. The design velocity for exterior surface nodes and interior nodes are computed separately based on a perturbation method. The sensitivity analysis is performed by both the direct differentiation and the adjoint variable method where special attention is given to periodic boundary conditions and verified by the forward finite difference method. The minimization of strain energy under p -norm von Mises stress constraint for Primitive sheet-based TPMS lattice structures produces an optimal non-uniform thickness distribution while keeping the cubic symmetric properties. Additional optimization results show that Primitive TPMS sheet lattice structure can achieve isotropy by varying its thickness distribution. The proposed shape optimization framework may not only be limited to elasticity application but fluid dynamics or thermal mechanics. The future work will take the transversely isotropic underlying material into consideration.

Reference

- [1] C.J. Ejeh, I. Barsoum, A.M. Abou-Ali, R.K. Abu Al-Rub, Combining multiple lattice-topology functional grading strategies for enhancing the dynamic compressive behavior of TPMS-based metamaterials, *J. Mater. Res. Technol.* 27 (2023) 6076–6093. <https://doi.org/10.1016/j.jmrt.2023.10.247>.
- [2] N. Yang, Z. Quan, D. Zhang, Y. Tian, Multi-morphology transition hybridization CAD design of minimal surface porous structures for use in tissue engineering, *Comput.-Aided Des.* 56 (2014) 11–21. <https://doi.org/10.1016/j.cad.2014.06.006>.
- [3] L. Zhang, Q. Ma, J. Ding, S. Qu, J. Fu, M.W. Fu, X. Song, M.Y. Wang, Design of elastically isotropic shell lattices from anisotropic constitutive materials for additive manufacturing, *Addit. Manuf.* 59 (2022) 103185. <https://doi.org/10.1016/j.addma.2022.103185>.
- [4] C.W. and D.E. Smith, Design of Spatially Varying Orientation Lattice Structures Using Triply Periodic Minimal, 2023 Int. Solid Free. Fabr. Symp. (2023). <https://par.nsf.gov/biblio/10507587-design-spatially-varying-orientation-lattice-structures-using-triply-periodic-minimal> (accessed August 20, 2024).
- [5] C. Wei, D.E. Smith, Spatially varying density and orientation for triply periodic minimal surface lattice design using topology optimization, *Int. J. Solids Struct.* 321 (2025) 113581. <https://doi.org/10.1016/j.ijsolstr.2025.113581>.
- [6] S. Daynes, Isotropic cellular structure design strategies based on triply periodic minimal surfaces, *Addit. Manuf.* 81 (2024) 104010. <https://doi.org/10.1016/j.addma.2024.104010>.
- [7] F. Günther, S. Pilz, F. Hirsch, M. Wagner, M. Kästner, A. Gebert, M. Zimmermann, Shape optimization of additively manufactured lattices based on triply periodic minimal surfaces, *Addit. Manuf.* 73 (2023) 103659. <https://doi.org/10.1016/j.addma.2023.103659>.
- [8] Q. Ma, L. Zhang, J. Ding, S. Qu, J. Fu, M. Zhou, M.W. Fu, X. Song, M.Y. Wang, Elastically-isotropic open-cell minimal surface shell lattices with superior stiffness via variable thickness design, *Addit. Manuf.* 47 (2021) 102293. <https://doi.org/10.1016/j.addma.2021.102293>.
- [9] Q. Ma, L. Zhang, M. Yu Wang, Elastically isotropic open-cell uniform thickness shell lattices with optimized elastic moduli via shape optimization, *Mater. Des.* 215 (2022) 110426. <https://doi.org/10.1016/j.matdes.2022.110426>.
- [10] P.J. Gandy, S. Bardhan, A.L. Mackay, J. Klinowski, Nodal surface approximations to the P, G, D and I-WP triply periodic minimal surfaces, *Chem. Phys. Lett.* 336 (2001) 187–195.
- [11] M.S. Flores-Jimenez, A. Delgado-Gutiérrez, R.Q. Fuentes-Aguilar, D. Cardenas, Generation of a Quadrilateral Mesh based on NURBS for Gyroids of Variable Thickness and Porosity, *J. Appl. Comput. Mech.* 8 (2022) 684–698.
- [12] T. DeRose, M. Kass, T. Truong, Subdivision surfaces in character animation, in: *Semin. Graph. Pap. Push. Boundaries Vol. 2*, 2023: pp. 801–810.
- [13] C. Le, J. Norato, T. Bruns, C. Ha, D. Tortorelli, Stress-based topology optimization for continua, *Struct. Multidiscip. Optim.* 41 (2010) 605–620.
- [14] Structural Sensitivity Analysis and Optimization 1: Linear Systems | SpringerLink, (n.d.). <https://link.springer.com/book/10.1007/b138709> (accessed April 7, 2025).
- [15] K.K. Choi, K.-H. Chang, A study of design velocity field computation for shape optimal design, *Finite Elem. Anal. Des.* 15 (1994) 317–341.
- [16] K.H. Huebner, D.L. Dewhirst, D.E. Smith, T.G. Byrom, *The finite element method for engineers*, John Wiley & Sons, 2001.
- [17] H. Si, TetGen, a Delaunay-Based Quality Tetrahedral Mesh Generator, *ACM Trans Math Softw* 41 (2015) 11:1-11:36. <https://doi.org/10.1145/2629697>.
- [18] K.M. Moerman, GIBBON: The Geometry and Image-Based Bioengineering add-On, . . GIBBON (2018).
- [19] K. Svanberg, The method of moving asymptotes—a new method for structural optimization, *Int. J. Numer. Methods Eng.* 24 (1987) 359–373.

- [20] C. Wei, D.E. Smith, Investigation of the Homogenized Anisotropy for the Triply Periodic Minimal Surface Lattice under Varying Applied Stress Orientation, (2024).